Supramolecular Photomagnetic Materials: Photoinduced Dimerization of Ferrocene-Based Polychlorotriphenylmethyl Radicals

Imma Ratera,[a] Daniel Ruiz-Molina,[a] José Vidal-Gancedo,[a] Juan J. Novoa,[b] Klaus Wurst,[c] Jean-François Letard,[d] Concepció Rovira,[a] and Jaume Veciana*[a]

Abstract: New ferrocenyl Schiff-base polychlorotriphenylmethyl radicals have been synthesized and characterized. The imino group of one such radical undergoes an irreversible *trans* to *cis* structural isomerization induced by light. Such photoinduced isomerization has been monitored by UV/Vis and ESR spectroscopy and also monitored by HPLC. ESR frozen solution experiments at low temperature revealed that the *cis* isomer dimerizes, showing a strong antiferromagnetic interaction. Although numerous photochromic supramolecular systems have been described, such a photoinduced self-assembly process represents the first example of a one-way photoswitchable magnetic system in which a conversion between a doublet and a singlet ground state species is promoted by a photoinduced dimerization process driven by the formation of hydrogen bonds. DFT calculations on the minimized structure and on the rotational barriers have been performed to establish the origin of such behavior. The effect of the substituents and the media polarity on the photoisomerization of this imine chromophore have also been studied. It has been observed that the efficiency of the process is markedly dependent on the presence and characteristics of electron-donor and electron-acceptor substituents of the ferrocenyl Schiff-base polychlorotriphenylmethyl radicals as well as on the polarity of the solvent.

Keywords: *cis–trans* isomerization · ferrocene · photomagnetism · self-assembly · triphenylmethyl radical

Introduction

There is currently great interest in the preparation of photomagnetic materials whose magnetic properties may be controlled by using light.[1,2,3] Such control of magnetic properties by optical stimuli may have applications in magneto-optical devices. Several examples of photomagnetic devices in i) inorganic magnetic systems, ii) covalently linked organic polyradicals, and iii) organic/inorganic magnetic systems, have already been described.[4,5,6] Indeed, Prussian Blue analogues are examples of inorganic photomagnetic systems in which long-range magnetic ordering is modified by photons.[7] Further examples of inorganic photoinduced magnetic systems are photoswitchable coordination compounds that interconvert reversibly between two isomers with different magnetic properties, such as spin-crossover[2,8] or valence tautomerism.[9] Different examples of photoinduced magnetization changes in purely organic materials have also been described. For instance, the photoisomerization of a carbene compound[10] or the spin isomerization of a non-Kekulé diradical are representative examples of such a kind of compounds.[11] More recently, Irie and Matsuda described an organic photochromic system that interconverts reversibly between a singlet and a triplet state.[12] Iwamura et al. have also reported a diradical species bearing two stable nitroxide radicals connected through an isomerizable unit.[13] The third family of photomagnetic molecular materials is composed of organic/inorganic hybrid systems where a magnetically active transition-metal ion is coordinated with a photoresponsive magnetic coupler.[14]

Even though several examples of molecular photomagnetic materials have been studied, to the best of our knowledge,

[a] I. Ratera, Dr. D. Ruiz-Molina, Dr. J. Vidal-Gancedo, Dr. C. Rovira, Prof. J. Veciana
Institut de Ciència de Materials de Barcelona (CSIC)
Campus Universitari de Bellaterra, 08193-Cerdanyola (Spain)
Fax: (+34) 93-5805729
E-mail: vecianaj@icmab.es

[b] Prof. J. J. Novoa
Departament de Química Física
Facultat de Química, Universitat de Barcelona
Av. Diagonal 47, 08208, Barcelona (Spain)

[c] Dr. K. Wurst
Institut für Allgemeine Anorganische und Teoretische Chemie
Universitat Innsbrück, 6020, Innrain 52a (Austria)

[d] Dr. J.-F. Letard
Institut de Chimie de la Matière Condensée (CNRS)
Château Brivazac, 87 Avenue du Docteur A. Schweitzer UPR
CNRS No. 9048, 33608 Pessac Cedex (France)

Supporting information for this article is available on the WWW under http://www.chemeurj.org/ or from the author.

 DOI: 10.1002/chem.200305194

there are no previous examples of supramolecular photomagnetic materials despite their enormous future potential. Indeed, supramolecular self-organization is considered very important for the development of functional materials. Accordingly, supramolecular photochromic materials, photovariable helical supramolecular structures for reversible optical data recording, and photoswitchable self-organized peptide systems have already been reported. In addition, the construction of ordered arrays of nanostructures by employing organic self-assembly techniques provide alternative strategies for the production of nanodevices.[15] From the magnetic point of view, the synthesis of supramolecular magnetic materials based on the self-assembly of *open-shell* molecules, have attracted much more interest.[16] The construction of such solids requires that the structural subunits exhibit noncovalent interactions that can be controlled in a predictable form and that are able to transmit efficiently the magnetic interaction. Up to now, the different types of noncovalent intermolecular interactions that have been used for such a purpose are hydrogen bonding,[17] $\pi\cdots\pi$ stacking,[18] transition-metal ligation,[19] and bridging of ion radicals by their counterions.[20] Among them, hydrogen bonding has emerged as a particularly useful and efficient supramolecular tool. Moreover, transmission of magnetic interactions through hydrogen bonds has been demonstrated to be quite efficient in metal complexes[21] and in several hydrogen-bonded organic magnets.[17] Despite the interest of having switchable magnetic materials, hydrogen-bonded supramolecular magnetic materials, whose properties may be systematically tuned and/or controlled by external stimuli, are limited to one example.[22] This compound, synthesized and studied by some of us, is the ferrocene-based polychlorotriphenylmethyl radical **1**.[22]

Abstract in Catalan: *Han estat sintetitzats i caracteritzats nous radicals policlorotrifenilmetílics connectats a una unitat de ferrocè mitjançant una base de Schiff. El grup imino d'un d'aquests radicals experimenta una isomerització estructural irreversible de* trans *a* cis *mitjançant la llum. Aquesta isomerització fotoinduïda ha estat seguida amb les tècniques d' UV/Vis, espectroscòpia de RPE així com també mitjançant cromatografia d' HPLC. L'espectre de RPE d'una solució congelada revel.la que L'isòmer* cis *dimeritza mostrant una forta interacció antiferromagnètica entre monòmers. Malgrat els nombrosos sistemes supramoleculars fotocròmics que han estat descrits fins ara, aquest procés d'autoassemblatge fotoinduït representa el primer exemple d'interruptor magnètic fotoinduït d'un sol sentit en el qual té lloc una conversió de doblet a singlet de L'espècie en estat fonamental promoguda per un procés d'autoassemblatge mitjançant la formació d'enllaços d'hidrogen. S'han realitzat càlculs de DFT de les estructures minimitzades i de les barreres rotacionals per tal de poder establir L'origen d'aquest comportament. També s'ha estudiat L'efecte dels substituents i de la polaritat del medi en la fotoisomerització d'aquests cromòfors d'imina. S'ha observat que L'eficiència del procés té una dependència molt marcada amb la presència de substituents electro donadors així com també amb la polaritat del dissolvent.*

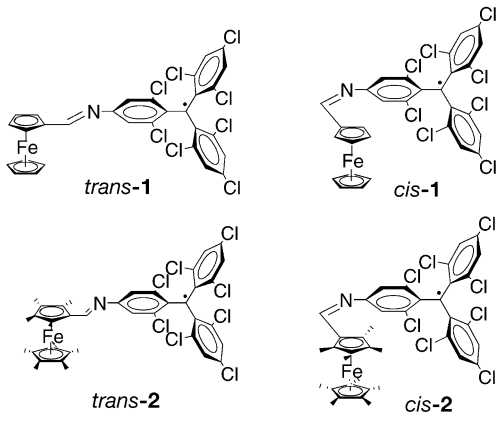

Here we report further studies with this ferrocene-based radical **1** as well as the nonamethylated ferrocenyl radical **2**. Both compounds are built up from three different units: the ferrocene unit, the polychlorotriphenylmethyl radical, and a connecting conjugated bridge. Such a conjugated bridge was designed to fulfill two main requirements: i) it should experience a reversible photoinduced structural change, such as a *trans–cis* photoinduced isomerization, and ii) it must promote the formation of supramolecular species through noncovalent interactions, such as hydrogen-bonding. Imino groups seemed to be excellent candidates as a photosensitive bridge since they are not only expected to exhibit a *trans/cis* photoisomerization but they might also induce the formation of weak hydrogen bonds. Another advantage of imino groups is their low thermal barrier for the interconversion between the two isomers. The relaxation from a photoinduced geometrical change in these imino compounds is extremely rapid and this feature may offer advantages for some light-driven devices. For instance, in 1977 Maeda and Fisher reported the photoinduced *trans/cis* isomerization of a number of *N*-benzilidenanilines and from experiments at $-70\,^{\circ}C$ they were able to characterize the thermally labile *cis* isomers.[23]

For the ferrocenyl imino radical **1**, two different isomeric forms were found and isolated, the *trans*-**1** and *cis*-**1** isomers. The *trans*-**1** isomer exists in solution as a monomeric species while the *cis*-**1** isomer dimerizes in solution forming a thermodynamically stabilized hydrogen-bonded diradical species, $(cis\text{-}\mathbf{1})_2$. Radical *trans*-**1** interconverts by irradiation into dimeric species $(cis\text{-}\mathbf{1})_2$, in which relatively strong antiferromagnetic interactions are developed. Finally, the nonamethylated ferrocenyl imino radical *trans*-**2** was also synthesized and its photochemical responses studied and compared with those found for the non-methylated radical *trans*-**1**.

Results and Discussion

Synthesis: The non-methylated ferrocenyl imino radical **1** was obtained by a condensation reaction between the ferrocene monocarboxaldehyde and the (4-amino-2,6-dichlorophenyl)-bis(2,4,6-trichlorophenyl)methyl radical (**4**;

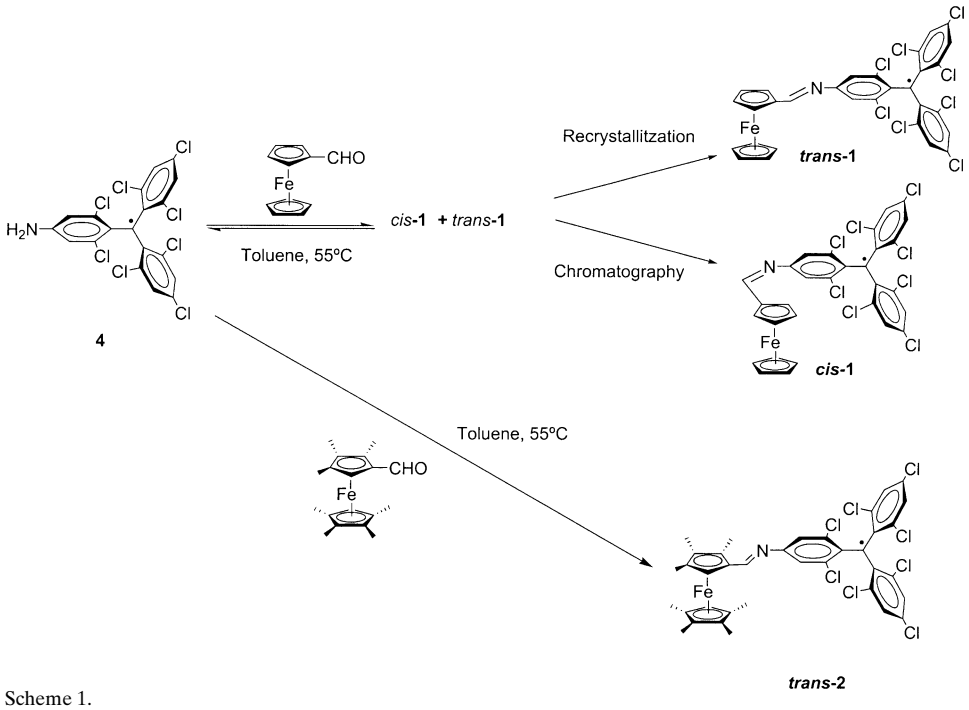

Scheme 1.

Scheme 1).[24] Since this condensation reaction is not stereoselective, the *trans* and *cis* isomers of compound **1** were formed in the reaction. Both isomeric forms, *trans*-**1** and *cis*-**1**, were isolated as stable species in solution and in the solid state. The *trans*-**1** isomer was isolated as a dark brown microcrystalline material by recrystallization from *n*-hexane, whereas the *cis*-**1** isomer was isolated as a dark green powder by flash chromatography. The nonamethylferrocenyl imino radical **2** was also obtained by means of a condensation of the amino-substituted radical **4** and the corresponding nonamethylferrocene monocarboxaldehyde (Scheme 1). In this case, the condensation takes place as for radical **1**, although the reaction rates are considerably slower. This fact is attributed to the deactivation of the nonamethylferrocene aldehyde in front of the nucleophilic attack of the amino radical group, due to the presence of deactivating methyl substituents. Moreover, it has to be emphasized that for radical **2**, only the *trans* isomer was isolated as a stable species. This fact has been attributed to high steric hindrance between the methyl groups of the ferrocene unit and the chlorine atoms of the triphenylmethyl radical in the *cis* configuration. Finally, compounds **1** and **2** were characterized by different techniques such as elemental analysis, LDI-TOF/MS, HPLC, cyclic voltammetry, FT-IR, UV/Vis-NIR, and ESR spectroscopies.

Physicochemical characterizations: *X-ray characterization*: Single crystals of *trans*-**1** were grown by slow evaporation of a carbon tetrachloride/hexanes (1:1) mixture and used for X-ray crystal determination.[25] It must be also emphasized that despite the recurrent use of different crystallization techniques and solvents, the obtaining of crystals suitable for the determination of the X-ray structure of the *cis*-**1** isomer[26] and *trans*-**2** remained elusive.

trans-**1** crystallizes in the monoclinic space group $P2_1/n$ with four molecules in the unit cell. The ORTEP plot of *trans*-**1** (Figure 1a) reveals almost eclipsed cyclopentadienyl rings, a *transoid* configuration of the CH=N unit and a propeller-like conformation of the polychlorinated triphenylmethyl unit. Despite the available resonance pathway and the *trans* configuration of the imino bridge, the cyclopentadienyl (Cp) ring and the $C_6H_2Cl_2$ ring are twisted by a dihedral angle of 28°. The lack of coplanarity may originate either from the presence of steric interactions between the hydrogen atom of the Cp ring and one of the *ortho*-hydrogen atoms of the triphenyl-

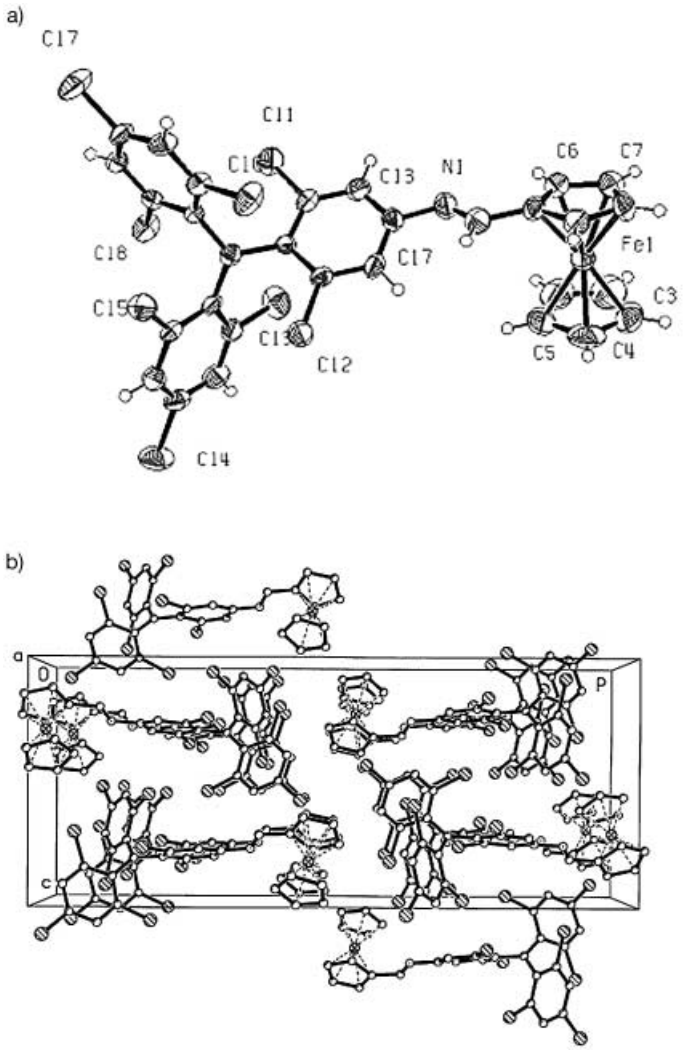

Figure 1. a) The structure of the radical *trans*-**1** (ORTEP molecular representation). b) Crystal packing of radical *trans*-**1**.

methyl unit and/or from the overlap between of the lone pair of electrons on the nitrogen atom and the π electrons of the triphenylmethyl unit.

The solid-state packing of *trans*-**1** (Figure 1b) is best described as centrosymmetrically-related pairs of molecules. Stacking of these related pairs occurs with continuous staggering along the *c* axis and with a head-to-tail pairing along the *b* axis. The relative arrangement and the large distances between neighboring molecules excludes the presence of hydrogen bonds among neighboring CH=N units. Under these circumstances, the largest driving forces for such molecular packing are van der Waals, π····π and short Cl···H–C interactions, which lead to efficient space filling.

Theoretical calculations: To rationalize the properties of the *trans* and *cis* isomers of radicals **1** and **2**, we decided to perform ab initio calculations to evaluate their structural and electronic properties. We have carried out UB3LYP calculations on the doublet ground state of the two isomers of radicals **1** and **2** using the LANL2DZ basis set, which uses the Wadt–Hay effective core potentials for the core electrons, while a basis set of double zeta quality is used for the outer electrons. The ground state is, for these radicals, the doublet state and presents a very small spin contamination at the UB3LYP/LANL2DZ level. The calculations were carried out using the crystal geometry of the *trans*-**1** isomer, while the optimum UB3LYP/LANL2DZ geometry of the doublet was used for all other isomers as no crystal structure is available for them. Figure 2 shows the optimized geometry of these three isomers along with the geometry of *trans*-**1** found experimentally. Table 1 collects the main structural parameters defining the relative disposition of the three main units of these radicals: the ferrocene, -C=N-, and polychlorinated triphenylmethyl groups. Interestingly, similar bond lengths and angles were found for the two isomers of each radical. Also worthy of note is the lack of planarity between the Cp ring of ferrocene and the $C_6H_2Cl_2$ ring connected to the bridging group. This lack of planarity, which is ascribed to steric hindrance, makes the overlap between the π orbitals of nearby units difficult, thus lowering the delocalization over the whole radical. As such non-planarity is found in the isolated radicals, it must be considered as an intrinsic property of the

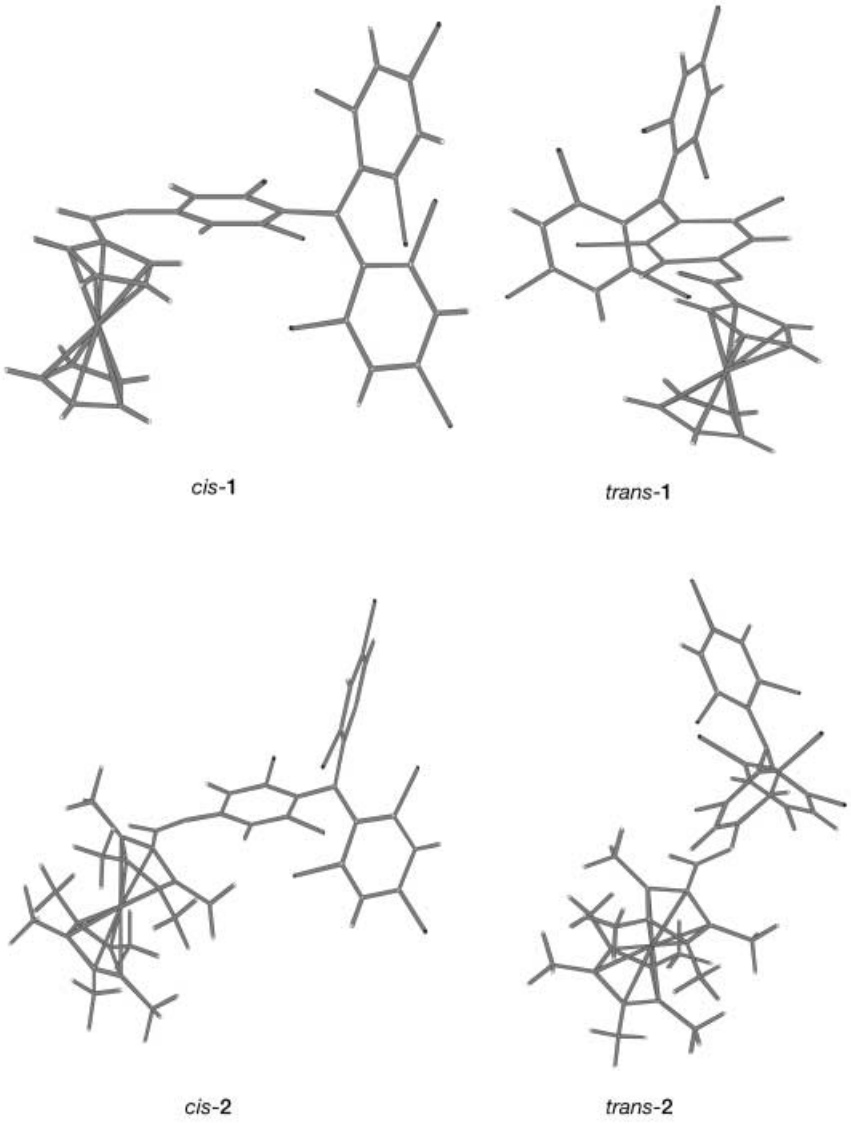

Figure 2. Minimized structures for the *cis*-**1**, *cis*-**2**, and *trans*-**2** isomers according to DFT calculations. For the *trans*-**1** isomer the crystal structure is shown.

Table 1. Main structural parameters describing the geometries of the *cis* and *trans* isomers of radicals **1** and **2**. Bond lengths [Å] and angles [°] and dihedral angles [°].

Radical	d_1[a]	d_2[b]	d_3[c]	α_1[d]	α_2[e]	γ_1[f]	γ_2[g]
trans-**1**	1.237	1.474	1.422	121.7	120.2	9.0	22.7
cis-**1**	1.237	1.475	1.421	121.7	120.2	14.6	27.9
trans-**2**	1.306	1.465	1.399	131.0	127.5	38.0	30.6
cis-**2**	1.309	1.465	1.401	130.9	127.3	37.9	36.9

[a] Bond length of N=C. [b] Bond length between C atoms of N=C–Cp. [c] Bond length between C and N atoms of N=C and triphenylmethyl units. [d] Bond angle between N=C–C(Cp). [e] Bond angle between -C=N-C($C_6H_2Cl_2$). [f] Dihedral angle between the Cp ring and the plane defined by N=C–C(Cp) atoms. [g] Dihedral angle between the $C_6H_2Cl_2$ ring and the plane defined by the N=C–C(Cp) atoms.

radicals, and not just being a consequence of intermolecular interactions in the crystal. Finally, the isomers of the nonamethylated radical **2** have similar structural parameters to those of the non-methylated ones, although it is worth mentioning the increase of 0.07 Å in the C=N bond, and the increased non-planarity between the three main units.

The electronic structure of studied radicals can be described by the shape and energetic distribution of the highest occupied (HOMO) and the lowest unoccupied (LUMO) molecular orbitals. Figure 3a shows the energetic distribution of these orbitals for the *cis*-**1** isomer which is nearly identical to that obtained for the *trans*-**1**, while the shape of these orbitals is depicted in Figure 4 for *cis*-**1** (see Figure S2 in the Supporting Information for the orbitals of *trans*-**1**). The energies of the four orbitals of Figure 3a are −0.20, 2× (−0.22), and −0.25 Hartrees. The single-occupied molecular orbital (SOMO) is mostly placed on the α-carbon atom (C_α) of the triphenylmethyl unit, with a small contribution on the

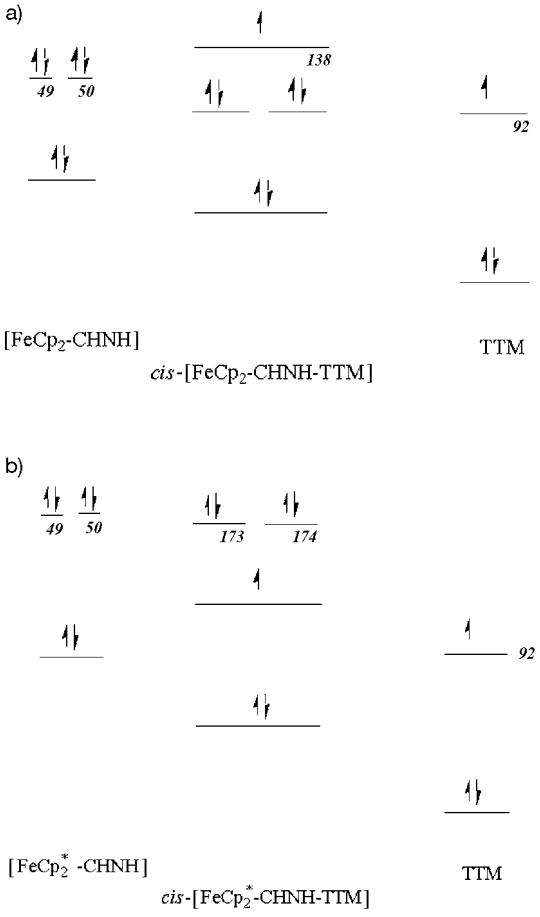

Figure 3. Qualitative partial molecular orbital diagrams of the studied radicals. a) *cis*-**1** radical showing the frontier orbitals of the ferrocene fragment and of the tris(trichlorophenyl)methyl (TTM radical) fragments at both sides. Orbitals 49 and 50 are the HOMO orbitals corresponding to the ferrocene fragment, 92 is the SOMO orbital of the TTM radical and 138 is the SOMO orbital formed for the corresponding *cis*-**1** isomer. b) *cis*-**2** radical showing the frontier orbitals. Orbitals 49 and 50 are the HOMO orbitals corresponding to the methylated ferrocene fragment, 92 is the SOMO orbital of the TTM radical, 173 and 174 are the HOMO orbitals formed for the corresponding *cis*-**2** isomer and 172 is the SOMO orbital where the unpaired electron resides.

six-membered ring attached to the C=N group, and also on the C=N group (see Figure 4). Below the SOMO, one finds two occupied molecular orbitals (HOMO-1 and HOMO-2), which are degenerate and placed on the Fe atom of the ferrocene unit. The LUMO is also located on the ferrocene unit, $FeCp_2$, with a small contribution on the C=N unit.

Figure 3b and Figure 5 show, respectively, the energy diagram and the shape of the frontier orbitals of the *cis*-**2** isomer (see Figure S3 in the Supporting Information for the frontier orbitals of *trans*-**2**). Once again, in the energy diagrams of the two isomers there is a one-to-one correspondence between the orbitals of *cis*-**2** and *trans*-**2** (not shown) compounds, their energies being 2×(−0.20), −0.21, and −0.22 Hartrees. The SOMO orbital is mostly located on the C_α atom of the triphenylmethyl fragment for both isomers. However, in the *trans*-**2** and *cis*-**2** isomers the doubly degenerate HOMO-1 and HOMO-2 orbitals sitting on the Fe atom of the nonamethylated ferrocene, $Fe(Cp^*)_2$ fragment are now energetically above the SOMO orbital. An energy diagram like that in Figure 3b corresponds to the ground state of this system, despite the fact that the SOMO orbital is not the highest in energy. The reason is that the orbital energy is not the only term in the Hartree–Fock or DFT energy.[27] The origin of the change in the relative stability of the SOMO orbital is double: a) a decrease in the stability of the $Fe(Cp^*)_2$ orbitals compared to the $Fe(Cp)_2$ orbitals (the relative ordering of the orbitals in $Fe(Cp^*)_2$ and $Fe(Cp)_2$ is the same, and so their energetic separation), and b) a decrease in the bonding–antibonding energy splitting for the combination of the tris(2,4,6-trichlorophenyl)methyl (TTM radical) and the HN=C orbitals. The second effect is induced by the increase in the non-planarity of these two units in the *trans*-**2** and *cis*-**2** isomers—notice the larger dihedral angles mentioned above.

As the studied systems have open-shell electronic structures it is interesting to know the spin distributions over the molecules. Consequently, we have computed for the four isomers studied here, in doublet ground states, the integrated spin density on each atom[28] according to the Mulliken population scheme,[29] and also the spin density and the hyperfine coupling constants on each nucleus. These are relevant parameters to understand the experimentally observed ESR hyperfine coupling constants. We have performed all these calculation on the experimental geometry or, when not available, on the optimized B3LYP/LANL2DZ geometry. The results, collected in Table 2 (see also Figure S4 in the Supporting Information), show that the spin density is mostly located on the C_α atom of the triphenylmethyl unit, with a small delocalization over the $Fe(Cp)_2$ unit in the *cis*-**1** case. This spin distribution is a consequence of the shape of the SOMO orbitals, though the spin map also indicates the presence of a small spin polarization on other atoms where the SOMO orbital has almost no weight. This is consistent with the integrated atomic spin populations, whose largest component is placed also on the C_α atom (see Table 2). Besides this, the integrated atomic spin populations show a sign alternation between neighboring atoms. It is interesting to note the small—but nonzero—amount of spin on the N and H atoms of the C=N unit.

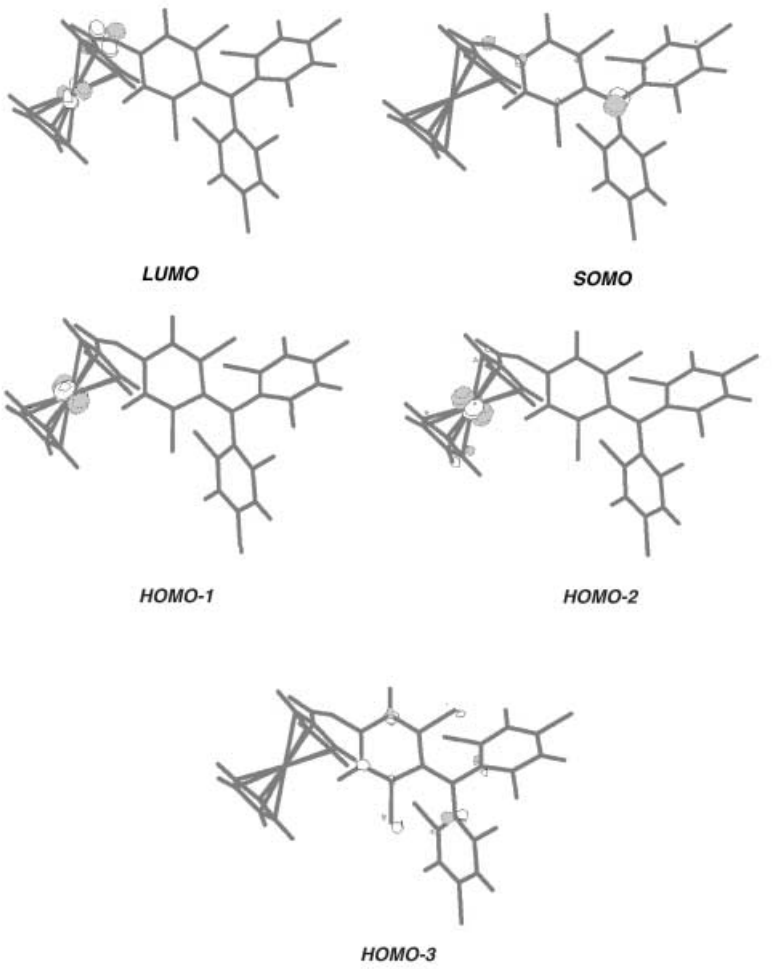

Figure 4. Molecular orbitals of *cis*-**1** according to DFT calculations.

Table 2. Integrated atomic spin populations (first row, in atomic units) and isotropic hfc constants (in Gauss, second row), of the most relevant nuclei, obtained by DFT calculations (see text).

Radical	C_α	C_{bridge}[a]	C_{ortho}[a]	N	H(C=N)
trans-**1**	+0.76	−0.12	+0.10	−0.02	−0.002
	+48.2	−15.3	+13.4	−0.18	−0.63
cis-**1**	+0.58	−0.12	+0.11	−0.01	−0.003
	+36.4	−14.3	+12.5	+2.18	−1.04
trans-**2**	+0.74	−0.12	+0.08	−0.01	−0.001
	+63.8	−13.4	+12.9	−0.02	−0.04
cis-**2**	+0.74	−0.11	+0.09	−0.01	−0.001
	+63.8	−13.6	+11.5	+0.42	−0.32

[a] The values for C_{bridge} and C_{ortho} are averaged over the three and six atoms that share such a condition.

To obtain out more information about the *trans/cis* isomerization process in these systems, we have also investigated the shape of the potential energy curve for the *trans–cis* isomerization of radicals **1** and **2**. For such a study we computed the optimum structure of the doublet ground state at various values of the dihedral angle θ-defined in the inset of Figure 6, which describes the relative arrangement of ferrocene, -C=N-, and triphenylmethyl units.[30] The potential energy curve computed after a full optimization of the geometry of the radical for each value of θ is shown in Figure 6 for radicals **1** and **2**.[31] The interconversion curves for both radicals are very similar and present only two minima, one for the *cis* and another for the *trans* isomer, separated by an energy barrier. In neither of the two minima are the ferrocene, bridge and phenyl units completely coplanar, while the maximum separating both minima occurs at a θ value of about 60°. Surprisingly, the energy barrier is not strongly influenced by the presence of the methyl groups in the ferrocene unit. In fact, it is only 5 kcal mol^{-1} smaller for **2** than for **1** due to the presence of a stabilizing CH···π interaction in compound **2**, an interaction that does not exist in compound **1**. In both cases the *trans* form is more stable than the *cis* isomer, the energy difference between them being very similar (4 and 6 kcal mol^{-1} for radicals **1** and **2**, respectively). In principle, the population of the *cis* and *trans* isomers at room temperature for both isomers of radical **1** and **2** should be very similar at least in the absence of significant solvent effects, or when these effects are not specific to one of the isomers.

Since one of the species involved in the *trans–cis* isomerization of radicals **1** and **2** exists in solution as a dimer (vide infra), we have also studied the energies involved in the dimerization of *cis* and *trans* isomers of radicals **1** and **2**. Figure 7 shows the optimized geometry found for the resulting dimer of the *cis*-**1** radical, using the AM1 semiempirical method. This dimer has C_2 symmetry with the two moieties arranged in a head-to-tail manner by means of two equivalent and complementary C–H···N H-bonds, with a H···N distance of 2.8 Å. Using the AM1-optimized geometry, we have done a B3LYP/LANL2DZ calculation of the interaction energy of the dimer. To lower the computational cost, the two external phenyl rings of both triphenylmethyl units were substituted by H atoms without relaxing the geometry of the dimer. The BSSE-corrected interaction energy of the dimer is −2.5 kcal mol^{-1}. This is a lowest energy limit (we have estimated using models that the effect of relaxing the geometry, and the inclusion of the external phenyl rings, which would allow the formation of new C–H···π bonds, would raise the interaction energy up to around −10 kcal mol^{-1}). The dimer is in a triplet electronic state and the two ferrocene groups of the two bonded molecules are in up-

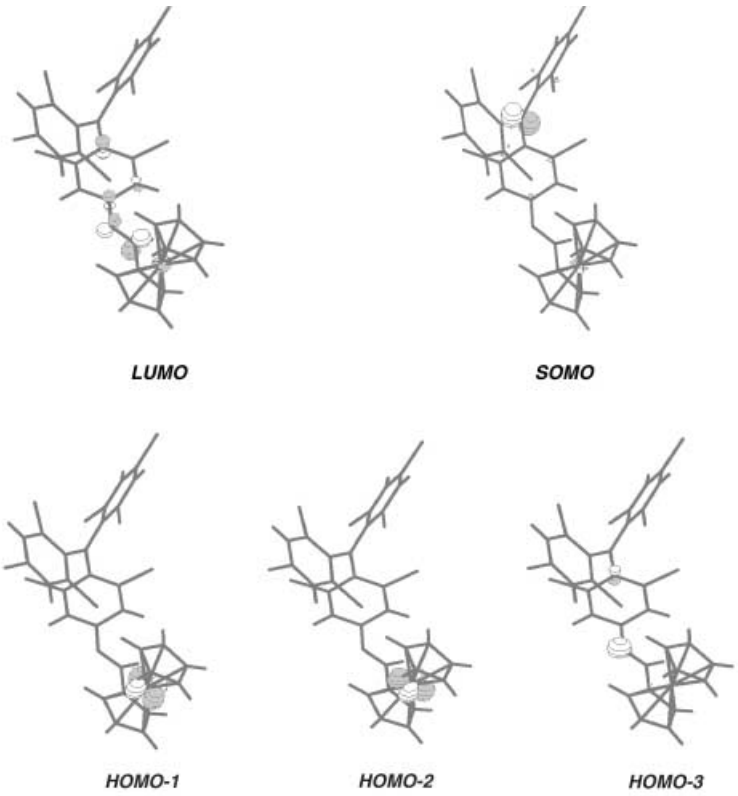

Figure 5. Molecular orbitals of *cis*-**2** according to DFT calculations.

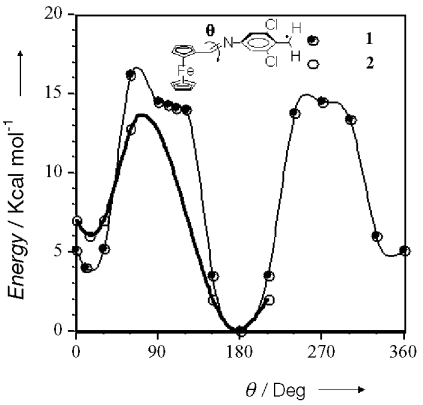

Figure 6. Calculated potential energy curves for the *trans/cis* interconversion of radicals **1** and **2**. Inset: Definition of the torsion angle θ from which the potential energy curve have been calculated.

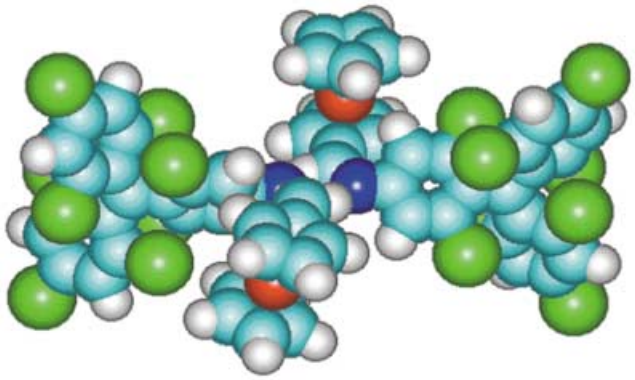

Figure 7. Optimized structure with AM1 semi-empirical methods of the supramolecular H-bonded dimeric (*cis*-**1**)$_2$ species formed by radical *cis*-**1**.

down positions with respect to the plane (reference plane) defined by the two bonded HC=N units, although the energy does not change significantly if both ferrocene groups are at the same side of the reference plane. In radical **2**, the steric hindrance makes the formation of (*cis*-**2**)$_2$ dimers very unstable energetically since short H···H contacts between the *meta*-H atoms of the triphenylmethyl units and the methyl groups of the Fe(Cp*)$_2$ units occurs. On the other hand, the specific geometries of the *trans* isomers of radicals **1** and **2** avoid the formation of dimers by means of two complementary C–H···N interactions. Thus, the only dimer that is energetically favored is the (*cis*-**1**)$_2$.

Interestingly, the optimized geometry obtained for *cis*-**1** at $\theta = 90°$, which has the three C–C=N atoms linearly arranged, is identical to that obtained at $\theta = 270°$ (see Figure S5 in the Supporting Information). This result proves that the isomerization process in this radical takes place through a mechanism that involves a semilinear geometry of the excited transition state with an inversion of the bond angle at the nitrogen atom in contrast with the isomerization mechanism of stilbene that isomerizes by an internal rotation about the ethylene bond angle.[32] A similar mechanism has been proposed for the isomerization of other imines derivatives.

UV/Vis-NIR spectroscopy: The absorption spectra of radicals **1** and **2** in CH_2Cl_2 are characterized by an intense absorption band at 377 nm with a shoulder at 420 and a weak band around 580 nm. For radical *trans*-**2** a very weak broad band at 800 nm was also observed. Table 3 gathers the most relevant data observed for radicals **1** and **2**. The bands at 377 and 580 nm are ascribed to radical chromophores since this kind of radical usually shows an intense absorption centered at 380 nm and two weaker bands cen-

Table 3. Relevant UV/Vis-NIR data obtained in CH_2Cl_2 solution at room temperature (λ, in nm; ε, in $M^{-1}cm^{-1}$).

Radical	λ_1 ($\varepsilon \times 10^{-3}$)	λ_2 ($\varepsilon \times 10^{-3}$)	λ_3 ($\varepsilon \times 10^{-3}$)	λ_4
5	386(28.2)	430(15.9)	567(1.5)	–
trans-**1**	377(22.0)	410(16.3)	563(1.5)	–
cis-**1**	377(28.6)	415(15.8)	584(3.9)	–
trans-**2**	378(3.2)	436(16.7)	593(5.6)	800(0.4)

tered around 565–605 nm. Consequently the band observed at 410 nm is unprecedented in unsubstituted polychlorinated triarylmethyl radicals and can be therefore ascribed either to intrinsic ferrocene transitions and/or, to the electronic delocalization of the unpaired electron into the π-conjugated system. Indeed, in the case of radicals **1** and **2**, due to the presence of a certain degree of electronic delocalization of the unpaired electron into the π-conjugated system, bathochromic shifts with enhanced absorptivities, compared to unsubstituted chlorinated triarylmethyl radicals, would be expected. Such behavior has already been observed for a related *p*-bromostyryl-substituted monoradical (**5**).[33] On the other hand, unsubstituted ferrocene exhibits two weak bands at 325 and 440 nm.[34] The shorter wavelength band is assigned to a Fe(dπ)→Cp(π*) charge transfer, or a π→π* transition, or a combination of these, whereas the longer wavelength is assigned to a d–d transition within the ligand field formalism. Upon substitution of one of the Cp rings of ferrocene with conjugated acceptors, one would expect changes of the visible spectra. Thus, even though the position and intensity of the ferrocene bands depends upon the nature of the chromophore acceptor group, shifts up to 520 nm and intensities of $\varepsilon = 1.0 \times 10^{+4}\,\mathrm{L\,mol^{-1}\,cm^{-1}}$ have been reported.

More interesting is the observation for radical *trans*-**2** of an extra broad band at around 800 nm ($\varepsilon = 360\,\mathrm{L\,mol^{-1}\,cm^{-1}}$) that is observed neither for substituted polychlorotriphenylmethyl radicals nor for substituted ferrocenes. In addition, such a band follows the Beer–Lambert law, a fact that indicates that this band has an intramolecular rather than intermolecular origin. Most likely, such a band may be assigned to an intervalence band transition[35] associated with an intramolecular electron transfer from the ferrocene unit to the radical unit, which have electron donor and acceptor character, respectively. On the other side, no intervalence band transition has been experimentally observed for radicals *trans*-**1** and *cis*-**1**. Why do we observe an intervalence transition exclusively for *trans*-**2**? One possible explanation of this fact is that the intervalence transitions for radicals *trans*-**1** and *cis*-**1** appear at higher energies as a very broad tail on the edge of a nearby electronic transition or even completely masked by it. Thus, the larger electron donor ability of the nonamethylated ferrocene unit for the *trans*-**2** isomer, decreases the energy difference between the HOMO and SOMO orbital, and consequently a decrease of the intervalence transition energy occurs. Therefore, an increase of the wavelength associated to this transition is expected. Moreover, the energetic orbital diagrams for radicals **1** and **2** indicate that one should find low energy excited states, particularly in the case of radical **2**. Besides, the small overlap that the HOMO and SOMO orbitals present in the region of the C=N bridge unit make feasible the existence of charge transfer states from the radical unit towards the ferrocene one.

Electrochemical studies: Cyclic voltammetric studies in CH_2Cl_2, with nBu$_4$NPF$_6$ (0.1 M) as supporting electrolyte (versus Ag/AgCl) and using Pt wire as a working electrode, were performed at room temperature (see Figure S8 in the Supporting Information). The cyclic voltammetric response of radicals *trans*-**1**, *cis*-**1**, and *trans*-**2** show two oxidation processes and one reduction process, all of them reversible. For radicals *trans*-**1** and *cis*-**1** the first oxidation process takes place at +0.61 and +0.72 V, respectively, and the second one at +1,05 V for both compounds, whereas the reduction process is observed at −0,66 and −0.67 V, respectively (versus an Ag/AgCl electrode in CH_2Cl_2). The cyclic voltammetric response of *trans*-**2** also show two reversible oxidation processes at +0.23 V and +1.12 V and one reversible reduction process at −0.60 V, respectively (versus an Ag/AgCl electrode in CH_2Cl_2). For the studied compounds, the first oxidation process arises from the oxidation of the ferrocene unit while the second reversible process is associated with oxidation of the triphenylmethyl radical unit to the corresponding carbocation. The reversible reduction process is associated with reduction of the triphenylmethyl radical unit to the corresponding carbanion, as ascertained by UV/Vis and ESR spectroelectrochemical experiments. The fact that the oxidation potential for the ferrocene units of radicals **1** and **2** appears at different potentials to those observed for ferrocene and decamethylferrocene provides evidence for the presence of an electronic interaction between the radical and the ferrocene units.[36]

Magnetic measurements: Variable-temperature magnetic susceptibility data have been collected for pure samples of *trans*-**1**, *cis*-**1**, and *trans*-**2** radicals in the temperature range of 2–300 K with an external field of 1 T. The effective magnetic moments found at room temperature for the three radicals were in excellent agreement with the theoretical effective magnetic moment expected for a simple ($S = 1/2$) monoradical ($0.37\,\mathrm{emu\,K^{-1}mol^{-1}}$). Then, the χT versus T plots give straight lines down to low temperatures where small downward deviations, due to the presence of weak intermolecular antiferromagnetic interactions, are observed.

For radicals *trans*-**1** and *trans*-**2**, the magnetic susceptibility data was nicely fitted to the Curie–Weiss law with Weiss constants of $\theta = -2.5$ and −2.1 K, respectively. Such small values are similar to those found for most polychlorotriphenylmethyl radicals reported up to now. However, in the case of radical *cis*-**1** the magnetic susceptibility data, depicted in Figure S9 in the Supporting Information, can be nicely fitted to a Curie–Weiss law characterized by a larger Weiss constant of $\theta = -15.3$ K. Experimental data can also be fitted to the Bleaney–Bowers model, which describes the behavior for a dimeric magnetic species, with an exchange coupling constant between unpaired electrons of $J/k_B = -18$ K using the Heisenberg Hamiltoninan formalism $\boldsymbol{H} = -2\,J\mathbf{S_1}\cdot\mathbf{S_2}$. Such a J value, which is unusually large for a member of this family of free radicals, may be tentatively attributed to presence of a relatively strong intermolecular antiferromagnetic interaction between the two radical moieties of the dimer, although the lack of an X-ray structure prevents us from knowing the precise arrangement of molecules in the solid state.

ESR spectroscopy: X-band ESR spectra of a toluene/dichloromethane (1:1) solution of radical *trans*-**1** ($c = 10^{-5}$ mol

L^{-1}) were obtained in the temperature range 160–300 K. At 300 K, the ESR spectrum shows a single central line without any apparent hyperfine structure, as occurs for most polychlorotriphenylmethyl radicals. To observe the hyperfine structure of this radical it was necessary to decrease the temperature down to 220 K. At this temperature, the ESR spectrum of radical *trans*-**1** (Figure 8a) shows several overlapped lines corresponding to the coupling of the unpaired electron with ^{1}H, ^{14}N, and naturally abundant ^{13}C isotopes at

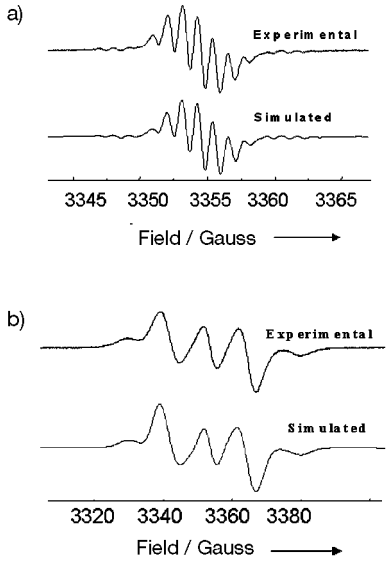

Figure 8. Experimental and simulated X-band EPR spectra of a toluene/CH_2Cl_2 (1:1) solution of a) *trans*-**1** at 220 K and b) *cis*-**1** at 160 K.

the alpha and aromatic positions of the triphenylmethyl unit. Computer simulation of the experimental spectrum gave an isotropic g value of $g_{iso}=2.0030$, which is very close to that observed for other polychlorotriphenylmethyl radicals,[37] and the hyperfine coupling constants (a_i): $a(^{14}N)=1.18$ G, $a(^{1}H_{trans})=0.25$ G, $a(^{13}C_{\alpha})=28.5$ G, $a(^{13}C_{bridge})=12.5$ G, $a(^{13}C_{ortho})=10.3$ G, $a(^{1}H_{meta})=1.06$ G.[38] These values are similar to those previously described for a related ferrocene-based polychlorotriphenylmethyl radical[39] and close to those theoretically determined by ab initio calculations, collected in Table 2. Finally, the spectrum of radical *trans*-**1** in a frozen solution at 160 K shows a slightly asymmetric broad single line that is characteristic of a free radical with a low magnetic anisotropy in a rigid medium. The absence of any fine structure under such conditions clearly shows that molecules of *trans*-**1** exists in solution as isolated, magnetically independent, species; that is as monomeric species.

The ESR spectrum of radical *trans*-**2** in a toluene/dichloromethane (1:1) mixture obtained at 220 K (see Figure S10 in the Supporting Information) was more complicated, since it shows an overall spectral asymmetry in spite of being recorded under isotropic conditions. Thus, such a spectrum consists of several overlapped lines, centered around a g value of 2.0037, that show distinct intensities and linewidths at both sides of the spectrum making it difficult to determine the experimental isotropic hfcc values. Such a spectral asymmetry is ascribed to the existence of a valence tautomerism phenomenon and in particular to the presence in solution of a thermally accessible doublet excited state involving a ferricinium cation, with an iron(III), and a carbanion on the triphenylmethyl unit. This charge-separated state is in equilibrium with another electronic isomer having a ferrocene unit, with iron(II), and the unpaired electron mostly localized at the triphenylmethyl unit. The presence of two species with slightly different g values in equilibrium might explain the observed spectral asymmetry for radical *trans*-**2**. This valence tautomerism seems to be favored in the case of radical *trans*-**2** because of the larger strength as electron donor of the nonamethylated ferrocene unit. This favors the intramolecular electron transfer from the $Fe(Cp^{*}_{2})$ to the radical center, that acts as an electron acceptor, forming the charge-separated species. In order to support this possible explanation, we computed such a charge-separated species by transferring the electron from the HOMO to the SOMO orbital. To lower the computational cost, we performed such a calculation on the small model of the *trans*-**2** radical used before in our calculations of the *cis–trans* potential energy curves.[30] At the optimum ground state geometry the HOMO→SOMO excited state lies 16.8 kcal mol^{-1} above the ground state energy, but after a geometry optimization, the excited state is just 4.4 kcal mol^{-1} above the optimum ground state energy, thus opening the door for a small thermal occupation of this state at room temperature. At the optimum geometry of the excited state the SOMO orbital is the LUMO orbital of the ground state (see Figure S7 in the Supporting Information). Such a change in the shape of the SOMO implies a charge transfer from the ferrocene to the triphenylmethyl radical unit. Consequently, there is an increase of the dipole moment of the excited state compared to the ground state value (their respective values are 9.2 and 5.9 Debye). The intramolecular electron transfer also affects the hfcc values since the hfcc of ^{57}Fe is smaller than 5.0×10^{-6} G in the ground state but it becomes 3.8×10^{-4} G in the excited state. The values of the atomic spin populations are also affected by the charge transfer since while in the ground state the electron is mostly located on the C_{α} atom of the triphenylmethyl unit (0.71 electrons) and almost no spin is found on the Fe atom of the ferrocene unit (0.09 electrons). In the excited state the situation is reversed and the C_{α} atom holds −0.57 electrons while 1.92 electrons are placed on the Fe atom. The valence tautomerism phenomenon proposed for radical *trans*-**2** in solution has been recently observed for a related ferrocene-based polychlorotriphenylmethyl radical in the solid state.[40] Further studies to fully confirm the existence of valence tautomerism for radical *trans*-**2** in solution are in progress.

More interesting results were obtained from the ESR spectrum of radical *cis*-**1**, in a toluene/dichloromethane (1:1) mixture at 220 K. Such a spectrum (Figure 8b) exhibits a fine structure, characteristic of a triplet species, instead of showing the hyperfine structure due to the coupling of magnetically active nuclei with the unpaired electron. The observation of a triplet species for *cis*-**1** is explained by the formation of a supramolecular dimeric species directed by intermolecular C–H···N hydrogen bonds between the -CH=N- groups of two different molecules oriented in a head-to-tail

manner similar to that depicted in Figure 7. As already mentioned in the theoretical calculation section, this dimeric structure has a C_2 symmetry and is stabilized with respect the monomer species by 10 kcal mol^{-1} because of the complementary H-bonds formed between head-to-tail oriented CH=N groups.Experimental zero-field splitting (zfs) parameters $|D'|$ and $|E'|$ determined from the frozen ESR spectrum, given in Gauss, provide information about the structure and electronic distribution of the H-bonded (*cis*-**1**)$_2$ species.[41] Thus, the zfs parameters obtained by a computer simulation of the spectrum obtained at 160 K were $|D'|=$ 25.2 G and $|E'|\cong 0$.[42] The null value determined for $|E'|$ suggests that the dimeric species has a quasi-axial symmetry, a result that is in agreement with the symmetry of the optimized structure of the dimer with the AM1 semiempirical method. Moreover, from the absolute value of the zfs parameter $|D/hc|$, given in cm^{-1}, and using [Eq. (1)],[43] an average interspin separation of 10.3 Å was found.

$$r = [\frac{3g^2\beta^2}{2hc}\frac{1}{|D/hc|}] \quad (1)$$

Such an averaged interspin separation is somewhat smaller than the nominal through-space separation of 14 Å between the two α-carbon atoms of two radical moieties determined from the optimized structure (Figure 7). This result is in agreement with the existence of a certain degree of spin delocalization over the imino bridges in the dimeric structure that reduces the effective separation of the two spins in the diradical species and, therefore, favor the presence of intermolecular magnetic exchange interactions.[44] The existence of (*cis*-**1**)$_2$ as a triplet species was confirmed by the observation of the forbidden $\Delta ms = \pm 2$ transition appearing at the half-field region of the spectrum. Its peak-to-peak intensity (I_{pp}) was measured in the 4–100 K temperature range. Since the experimental value of $I_{pp}T$ is proportional to the population in the triplet state, the fact that $I_{pp}T$ decreases with decreasing temperature indicates that the ground state of the dimeric species is in the singlet state while the triplet should be associated with a thermally accessible excited state. A separation of 54 ± 2 K (38 cm^{-1}) between both states was obtained from the fitting of the experimental data to a Bleaney–Bowers equation.[45] This value corresponds to an intermolecular exchange coupling of $J/k_B = -27$ K, which is close to that observed in the solid state (see Magnetic Measurements Section). The small difference could be explained by differences in the geometries of the H-bonded (*cis*-**1**)$_2$ dimer in solid and in solution produced by the solvent molecules.

Towards the development of a photomagnetic supramolecular device: The interconversion between the *trans*-**1** isomer, which exists in solution as a monomeric species, and *cis*-**1**, which spontaneously aggregates in solution generating the H-bonded (*cis*-**1**)$_2$ dimer, is important for the development of a new kind of photomagnetic supramolecular device. For this reason we performed a detailed study of the photochemically and thermally induced interconversions of radical **1** monitoring the changes with ESR and UV/Vis spectroscopy.

Photochemically induced isomerization: Methylcyclohexane was initially chosen as a solvent for this study because it makes a good glass when it is frozen at low temperature, avoiding the scattering of the light used for irradiation. At the same time, the high viscosity of the medium at low temperature hinders the mobility and tumbling of the species permitting, therefore, the observation of the ESR fine structure of triplet species produced by the dipolar interaction between the two unpaired electrons. Furthermore, methylcyclohexane is a nonpolar solvent that generally disfavors those intermediates showing a high polarity. The ESR spectrum of *trans*-**1** in frozen methylcyclohexane exhibited a time dependence behavior under in-situ irradiation at 415 nm,[46] with the appearance of spectral features that are consistent with the conversion from the *trans*-**1** to the (*cis*-**1**)$_2$ (see Figure 9). After eight hours of irradiation a mixture with a *cis*:*trans* ratio of 90:10, as confirmed by computer simulation, was obtained.

The photoinduced *trans*-**1** to *cis*-**1** isomerization in methylcyclohexane at room temperature was also monitored by UV/Vis spectroscopy. Indeed, both *trans*-**1** and *cis*-**1** isomers show two absorption bands at 377 and 410 nm that are ascribed, as already mentioned, to the radical and the conjugated ferrocene chromophores, respectively. The main difference between the two isomers lies in the relative intensity of both bands. In the case of the *trans*-**1** isomer, the band at 377 nm exhibits a lower absortivity, whereas the band at 408 nm exhibits a higher absortivity than those reported for the *cis*-**1** isomer.[47] These changes also allowed us to study the effect of irradiation upon a solution of *trans*-**1** in methylcyclohexane by absorption spectroscopy. Thus, the in situ irradiation of *trans*-**1** was carried out using a 415 nm light in a quartz cell at room temperature for 2 h. During the irradiation of the *trans*-**1** solution, the absorption of the band at 377 nm increased whereas that of the band at 408 nm decreased with the appearance of an isosbestic point at 382 nm confirming a neat transformation from the *trans*-**1** to the *cis*-**1** isomer. It must be emphasized that irradiation of a *cis*-**1** solution in methylcyclohexane with different wavelengths (415,

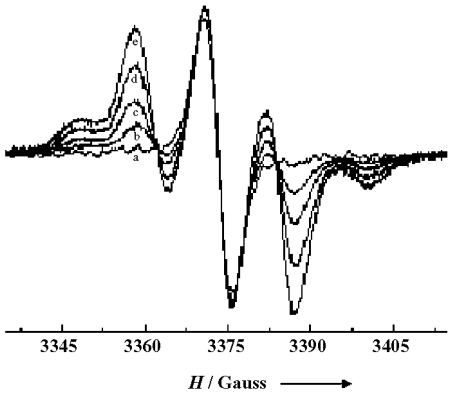

Figure 9. Photoinduced *trans*→*cis* isomerization of radical *trans*-**1** in a methylcyclohexane solution monitored by ESR spectroscopy. Spectra were taken after irradiating the sample for: a) $t=0$, b) 1, c) 3, d) 5, and e) 8 h.

380, 540 nm) did not lead to the reverse photoisomerization process, as observed by using ESR and UV-Vis spectroscopy. The stability of (*cis*-**1**)$_2$ species under irradiation is ascribed to the unfavorable energy requirements associated with its conversion into the *trans* isomer. It is well know that the efficiency of a *trans–cis* isomerization is markedly dependent on the polarity of the solvent. For this reason we also studied the isomerization of *trans*-**1** in solvents with larger polarities, like toluene and dichloromethane, observing that *trans*-**1** is photoinactive in both solvents. In marked contrast to the *trans*-**1** derivative, the irradiation at 415 nm of *trans*-**2**, both in nonpolar and polar solvents, did not exhibit any sign of isomerization.

In summary, the *trans*-**1** derivative is photoactive but only in nonpolar media, whereas both the *cis*-**1** and *trans*-**2** derivatives do not exhibit any photoinduced change either in non-polar or polar solvents. These results may be explained for *trans*-**1** if two alternative pathways with a common excited state, *trans*-**1***, like those shown in Scheme 2, are operative.[48] One such pathway is favored in non-polar media and leads to an efficient *trans* to *cis* conversion while the other pathway involves a charge-separated intermediate that reverts rapidly into the starting *trans* isomer avoiding the conversion to the *cis* isomer. The latter pathway is preferential in polar media and for those compounds having strong electron donor and acceptor groups linked to the isomerizable unit. Consequently, only the compound with the weaker electron-donor group (here the ferrocene) and held in solvents of low polarity shows a considerable photoactivity.

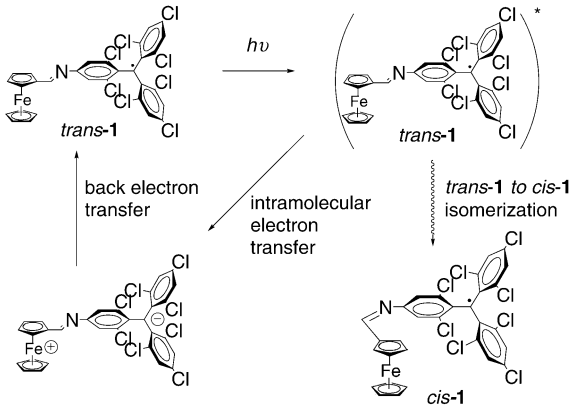

Scheme 2. The photoactivity of *trans*-**1**.

Thermally induced interconversion: The thermally induced isomerization process from t*rans*-**1** to *cis*-**1** has also been studied in three different solvents having distinct polarities, such as acetonitrile, toluene, and methylcyclohexane. Initially, a degassed solution of *trans*-**1** was warmed up to 80 °C and its evolution over time was monitored by HPLC chromatography and UV/Vis spectroscopy. The experimental results confirmed that, independently of the solvent used and in the absence of light irradiation, the thermally induced t*rans*-**1**→*cis*-**1** isomerization takes place. As an example, the evolution over time of an acetonitrile solution of *trans*-**1** at 80 °C, as monitored by HPLC, is shown in Figure 10. The initial chromatogram shows only the characteristic peak of the *trans*-**1** isomer. In the second chromatogram, obtained after approximately one hour, the intensity of the peak corresponding to the *trans*-**1** form decreases whereas the intensity

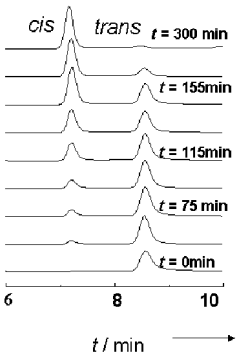

Figure 10. Evolution of the conversion of isomer *trans*-**1** in acetonitrile at 80 °C, as monitored by HPLC.

of a new peak, appearing at a lower retention time, that corresponds to the *cis*-**1** isomer increases. Such a trend continues with time and after five hours, a mixture with a *cis*-**1**:*trans*-**1** ratio of 95:5 is obtained. We have also examined the thermal behavior of a pure sample of *cis*-**1** at 80 °C in the same three solvents (methylcyclohexane, toluene and acetonitrile) but no evidence of a thermally induced backward *cis*-**1** to *trans*-**1** isomerization was observed. Thus, as summarized in Scheme 3, the *trans*-**1** to *cis*-**1** isomerization process takes place thermally while the reverse process do not takes place in any of the three studied solvents.[49]

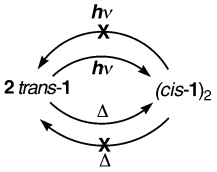

Scheme 3. *cis*-**1**→*trans*-**1** isomerization.

The irreversibility of this one-way photoinduced isomerization process has been attributed to the stabilization of radical *cis*-**1** in solution due to the formation of the thermodynamic stable H-bonded dimeric (*cis*-**1**)$_2$ species, as confirmed by theoretical DFT calculations and experimental spectroscopic evidence.

Conclusion

In summary both the *trans* and *cis* isomers of radical **1** have been isolated, whereas only the *trans* isomer of the nonamethylated derivative **2** can be isolated. Interestingly, the *cis*-**1** isomer aggregates in solution at low temperatures generating the thermodynamically stabilized H-bonded diradical

(*cis*-**1**)$_2$ species, in which strong antiferromagnetic interactions develop. The head-to-tail arrangement of the radicals and the spin density on the bridge HC=N unit are responsible for the presence of antiferromagnetic interactions. It is clear that the existence of a certain degree of delocalization over the imino bridge enhances the presence of magnetic exchange interactions between the two radical moieties. Due to high steric hindrance the corresponding dimer of the *cis*-**2** radical cannot be formed.

Photoinduced *trans*-**1**→*cis*-**1** isomerization has been shown to take place but only in apolar solvents. On the contrary, irradiation of a *cis*-**1** solution at different wavelengths did not provide any evidence about the presence of a backward photoisomerization processes. This one-way photoinduced self-assembly process represents an interesting example of a photomagnetic system based on a supramolecular phenomenon in which a doublet species is converted into a singlet one. This concept might be extended to the synthesis of novel compounds bearing other organic and inorganic magnetic units providing valuable access to this interesting class of supramolecular magnetic materials with which interesting supramolecular devices could be achieved.

Experimental Section

Computational methodologies: The minimization of the geometries of radicals **1** and **2** and the molecular orbital calculations were carried out at the UB3LYP level on the doublet ground state of the four isomers using the LANL2DZ basis set (which uses the Wadt–Hay effective core potentials for the core electrons, while a basis set of double zeta quality was used for the outer electrons). The doublet state for these radicals is the ground state and presents a very small spin contamination at the UB3LYP/LANL2DZ level. The calculations were done on the crystal geometry of the *trans*-**1** isomer, while the optimum UB3LYP/LANL2DZ geometry of the doublet was used for all other three isomers,[50] as no crystal structure was available for them. In the initial input geometries the N=C bridge and the phenyl and Cp rings of the ferrocene unit were kept planar; the dihedral angles defined by the N=C bridge and the phenyl and Cp rings were set to 0°. Moreover, for each radical, two different initial input conformations differing by a 180° rotation around one of the single bonds that connects the phenyl unit and the C=N unit were used. It is important to note that independent of the input model used, the minimized geometries converged in similar close-lying minima.

Starting materials: All solvents were reagent grade from SDS and were used as received or otherwise distilled as indicated. All reagents, organic and inorganic, were of high purity grade and obtained from E. Merck, Fluka Chemie, and Aldrich Chemical Co.

Experimental methodologies: Elemental analyses were obtained in Servei d'Anàlisis de la Universitat Autònoma de Barcelona (UAB). The MALDI/TOF mass spectrometer used was an Analytical Kompact LDI II from Kratos operating in positive mode and high power. Electrochemical experiments were performed with an EG and PAR potenciostat/galvanostat, using a Pt wire as working electrode and an Ag/AgCl electrode as reference electrode. Anhydrous CH_2Cl_2 freshly distilled over P_2O_5 under nitrogen was used as a solvent and tetrabutylammonium hexafluorophosphate (Fluka, electrochemical grade) as the supporting electrolyte. EPR spectra were recorded on a Bruker ESP-300E spectrometer operating in the X-band (9.3 GHz). Signal-to-noise ratio was increased by accumulation of scans using the F/F lock accessory to guarantee a high-field reproducibility. Precautions to avoid undesirable spectral line broadening such as that arising from microwave power saturations and magnetic field over-modulation were taken. To avoid dipolar broadening, the solutions were carefully degassed three times using vacuum cycles with pure Ar. The g values were determined against the DPPH standard ($g=2.0030$). To obtain accurate temperature measurements between 4 and 100 K that ensure the validity of the experimental results, the spectrometer was equipped both with a flowing-helium Oxford EPR-900 cryostat, controlled by an Oxford ITC4 temperature control unit, and with a calibrated custom-made double temperature control system for accurately determining the sample temperature. The program used to simulate the spectra were Win-EPR from Bruker (Germany) and Sinfonia v.1.0 from Bruker Instruments Billerca, MA (USA). Direct current (dc) magnetic susceptibility measurements were carried out on a Quantum Design MPMS SQUID susceptometer with a 55 kG magnet and operating in the range of 4–320 K. All measurements were collected in a field of 1.0 T. Background correction data were collected from magnetic susceptibility measurements on the holder capsules. Diamagnetic corrections estimated from the Pascal contents were applied to all data for determination of the molar paramagnetic susceptibilities of the compounds. HPLC chromatography was performed on a LC10-A Series Shimadzu spectrophotometer equipped with a diode array detector ($\lambda=250$–800 nm), an external computer and a Perkin Elmer Series pump system. The inverse phase chromatographic columns were ODS-2 of Teknokroma. X-ray data collection: Nonius Kappa CCD diffractometer with an area detector and graphite-monochromized $Mo_{K\alpha}$, radiation ($\lambda=0.7106$ Å). Cell constants were derived from the least-squares fit to the setting angles for 25 selected reflections with $10°\leq\theta\geq15°$. The structures were solved and refined using the SHELL-93 software and the measured reflections were corrected with the program Scaalepack. UV-Vis-NIR spectra were recorded using a Cary 5E Varian spectrophotometer. IR spectra were recorded using a Perkin Elmer spectrum one FT-IR spectrometer. The photochemical *trans*→*cis* isomerizations were followed by UV/Vis spectroscopy and supported by HPLC analysis. The UV/Vis in situ irradiation followed with a UV/Vis spectrometer were preformed with a 150 W xenon arc-lamp filtering the light through a monochromator set at a wavelength close to the absorption maximum of the chromophore. In situ irradiation experiments with the ESR technique were performed with a power of 10 mW cm^{-2} using a fiber optic illuminator Oriel model 77501, that uses a quartz tungsten halogen lamp, and various interference filters, centered from 350 to 450 nm.

Preparation of (*trans*)-4-(ferrocenylimino)bis(2,4,6-trichlorophenyl)-2,6-dichlorophenyl methyl radical (*trans*-1) and (*cis*)-4-(ferrocenylimino)-bis(2,4,6-trichlorophenyl)-2,6-dichlorophenyl methyl radical (*cis*-1): Ferrocene monocarboxaldehyde (80 mg, 0.37 mmol) was added to a dry solution of (4-amino-2,6-dichlorophenyl)bis(2,4,6-trichlorophenyl)methyl radical (200 mg, 0.37 mmol) in toluene, which was obtained as previously described,[24] over molecular sieves. The mixture was heated up to 60 °C and stirred for 48 h in the dark. The reaction was monitored by silica thin layer chromatography first eluted with a 5% TEA solution of 75% tetrachloride and 25% *n*-hexane. After removing the molecular sieves and evaporation of the solvent, a brown precipitate was obtained. This condensation reaction is not stereoselective so the reaction products contain a mixture of *cis* and *trans* isomers of compound **1**. The *trans*-**1** isomer (50 mg) was isolated in 20% yield as a dark brown microcrystalline material by recrystallization from *n*-hexane. The *cis*-**1** isomer (15 mg) was isolated in 6% yield as a dark green powder by flash chromatography, eluted with carbon tetrachloride, on a Florisil (magnesium silicate) column.

***trans*-1**: Elemental analysis calcd (%) for $C_{30}H_{16}Cl_8FeN$: C 49.4, H 2.21, N 1.90; found: C 49.6, H 1.8, N 2.0; IR (KBr): $\tilde{\nu}_{max}=3420$, 2967, 2913, 1631, 1556, 1536, 1465, 1371, 1261, 1225, 1182, 1137, 1104, 1021, 858, 809 cm^{-1}, UV/Vis (methylcyclohexane): λ_{max} (ε): 377 (20300), 409 (14900), 565 nm (1863 mol^{-1} dm^3 cm^{-1}); cyclic Voltammetry: −0.661 V, +0.609 V, and +1.054 V versus Ag/AgCl; EPR (isotropic solution of toluene at 220 K): $g=2.0030$; hyperfine coupling constants: a(N) = 1.1837 G; $a(^1H_{meta})=1.0569$ G; $a(^1H_{trans})=0.2453$ G; $a(^{13}C_{\alpha})=28.5$ G; $a(^{13}C_{bridge})=12.5$ G, and $a(^{13}C_{ortho})=10.3$ G; reverse-phase HPLC: $T=25$ °C; mobile phase: AcCN/THF; 70/30; flow: 1 mL min^{-1}, detectors at 220, 377, and 590 nm: one peak at 7.9 min; MS-LDI-TOF (positive-mode): m/z/uma/e$^-$ [$M^{+\cdot}$]: 729 [M]$^+$, 694 [$M-35$]$^+$, 659 [$M-70$]$^+$, 533 [$M-196$]$^+$.

***cis*-1**: Elemental analysis calcd (%) for $C_{30}H_{16}Cl_8FeN$: C 49.4, H 2.21, N 1.90; found: C 49.8, H 2.0, N 2.2; IR (KBr): $\tilde{\nu}_{max}=3434$, 2925, 2849, 1715, 1631, 1552, 1526, 1487, 1383, 1371, 1292, 1227, 1182, 1134, 1076, 1057, 926, 858, 817, 788 cm^{-1}; UV/Vis (methylcyclohexane): λ_{max} (ε): 377 (23300), 407 (13600), 578 nm (2940 mol^{-1} dm^3 cm^{-1}); cyclic voltammetry:

−0.669 V, +0.723 V, and +1.056 V versus Ag/AgCl; EPR (isotropic solution of toluene at 160 K): zero field splitting parameters: $|D'|=25.2$ G, $|E'|=0$; reverse-phase HPLC: $T=25$°C; mobile phase: AcCN/THF; 70/30; flow:1 mL min^{-1}; detection at 220, 377, and 590 nm one peak at 6.7 min; MS-LDI-TOF (positive mode): m/z/uma/e$^-$ [$M^{+\cdot}$]: 729 [M]$^+$, 694 [$M-35$]$^+$, 659 [$M-70$]$^+$, 533 [$M-196$]$^+$.

Preparation of the (*trans*)-4-(nonamethylferrocenylimino)-2,6-dichlorophenyl)bis(2,4,6-trichlorophenyl) methyl radical (2): Nonamethylferrocene monocarboxaldehyde[51] (318 mg, 0.936 mmol) was added to a dry toluene solution of (4-amino-2,6-dichlorophenyl)bis(2,4,6-trichlorophenyl)methyl radical (500 mg, 0.936 mmol), which was obtained as previously described,[24] over molecular sieves. The mixture was heated up to 60°C and stirred for 24 h in the dark. The reaction was monitored by silica thin layer chromatography first eluted with a 5% TEA solution of 75% tetrachloride and 25% *n*-hexane. After removing the molecular sieves and evaporation of the solvent, a brown precipitate was obtained. The resulting solid was purified with basic Al_2O_3 chromatography, using carbon tetrachloride as eluent, yielding pure *trans*-**2** (160 mg: 20% yield) as a dark brown microcrystalline powder.

***trans*-2**: Elemental analysis calcd (%) for $C_{39}H_{34}Cl_8FeN$: C 54.7, H 3.97, N 1.63; found C 54.48, H 4.48, N 1.73; IR (KBr): $\tilde{\nu}_{max}=3435$, 2923, 2850, 1716, 1631, 1555, 1523, 1454, 1370, 1288, 1183, 1137, 1075, 1024, 857, 809, 562 cm^{-1}; UV/Vis (CH_2Cl_2): λ_{max} (ε): 378 (31200), 593 (5600), 800 nm (400 mol^{-1} dm^3 cm^{-1}); cyclic voltammetry: −0.59 V, +0.233 V, +1.121 V versus Ag/AgCl; MS-LDI-TOF (positive mode): m/z/uma/e$^-$ [M]$^+$: 935 [M]$^+$, 900 [$M-35$]$^+$, 865 [$M-70$]$^+$.

Acknowledgments

We thank the Programa Nacional de Materiales, under project MAGMOL (MAT2003-04699), Ministerio de Ciéncia y Tecnología (Project BQU2002-0433-C02-01 and BQu2002-04587-C02-02), and DGR, Catalunya (2001SGR00362 and 2001SGR0044). Computer time allocated by CESCA/CEPBA and the CEPBA-IBM Research Institute is also acknowledged. I. R. thanks the Generalitat de Catalunya for a doctoral grant and the ESF Network Molecular Magnets.

[1] a) M. Verdaguer, *Science* **1996**, *272*, 698.
[2] a) P. Gütlich, A. Hauser, H. Spiering, *Angew. Chem.* **1994**, *106*, 2109; *Angew. Chem. Int. Ed. Engl.* **1994**, *33*, 2024 and references therein; b) K. Nagai, T. Iyoda, A. Fujishima, K. Hashimoto, *Solid State Commun.* **1997**, *102*, 809.
[3] S. Nakatsuji, M. Mizumoto, A. Takai, H. Akutsu, J. Yamada, H. Kawamura, S. Schmitt, K. Hafner, *Mol. Cryst. Liq. Cryst.* **2000**, *348*, 1.
[4] a) K. Hamachi, K. Matsuda, T. Itoh, H. Iwamura, *Bull. Chem. Soc. Jpn.* **1998**, *71*, 2937; b) K. Matsuda, M. Irie, *Chem. Lett.* **2000**, 16; c) K. Matsuda, M. Irie, *Tetrahedron Lett.* **2000**, *41*, 2577.
[5] a) S. Nakatsuji, Y. Ogawa, S. Takeuchi, H. Akutsu, J. Yamada, A. Naito, K. Sudo, N. Yasuoka, *J. Chem. Soc. Perkin Trans. 1* **2000**, *2*, 1969; b) T. Ojima, H. Akutsu, J. Yamada, S. Nakatsuji, *Chem. Lett.* **2000**, *918*; c) S. Takeuchi, Y. Ogawa, A. Naito, K. Sudo, N. Yasuoka, H. Akutsu,, J. Yamada, S. Nakatsuji, *Mol. Cryst. Liq. Cryst.* **2000**, *345*, 167.
[6] a) K. Matsuda, M. Irie, *J. Am. Chem. Soc.* **2000**, *122*, 7195; b) K. Matsuda, M. Irie, *J. Am. Chem. Soc.* **2000**, *122*, 8309; c) T. Ojima, H. Akutsu, J. Yamada, S. Nakatsuji, *Polyhedron* **2001**, *20*, 1335; d) S. Karasawa, N. Koga, *Polyhedron* **2001**, *20*, 1387.
[7] a) O. Sato, T. Iyoda, A. Fujishima, K. Hashimoto, *Science* **1996**, *272*, 704; b) V. Escax, A. Bleuzen, C. Cartier dit Moulin, F. Villain, A. Goujon, F. Varret, M. Verdaguer, *J. Am. Chem. Soc.* **2001**, *123*, 12 536.
[8] a) Renz, H. Oshio, V. Ksenofontov, M. Waldeck, H. Spiering, P. Gütlich, *Angew. Chem.* **2000**, *112*, 3832; *Angew. Chem. Int. Ed.* **2000**, *39*, 3699; c) P. Gütlich, Y. García, T. Woike, *Coord. Chem. Rev.* **2001**, *219–221*, 839.
[9] D. Ruiz-Molina, J. Veciana, K. Wurst, D. N. Hendrickson, C. Rovira, *Inorg. Chem.* **2000**, *39*, 617.
[10] W. Sander, G. Bucher, F. Reichel, D. Cremer, *J. Am. Chem. Soc.* **1991**, *113*, 5311.
[11] L. C. Bush, R. B. Heath, J. A. Berson, *J. Am. Chem. Soc.* **1993**, *115*, 9830.
[12] a) K. Matsuda, M. Irie, *Tetrahedron Lett.* **2000**, *41*, 2577; b) K. Matsuda, M. Irie, *Chem. Lett.* **2000**, 16.
[13] K. Hamachi, K. Matsuda, T. Itoh, H. Iwamura, *Bull. Chem. Soc. Jpn.* **1998**, *71*, 2937.
[14] S. Karasawa, H. Kumada, N. Koga, H. Iwamura, *J. Am. Chem. Soc.* **2001**, *123*, 9685.
[15] S. De Feyter, A. Gesquière, K. Wurst, D. B. Amabilino, J. Veciana, F. C. De Schryver, *Angew. Chem.* **2001**, *113*, 3317; *Angew. Chem. Int. Ed.* **2001**, *40*, 3217.
[16] a) *Magnetic Properties of Organic Materials* (Ed.: P. M. Lahti), Marcel Dekker, NY, **1999**, Academic, Dordrecht, **1999**; b) *Magneto Science: Molecules to Materials Vols. 1 and 2* (Eds.: J. Miller, M. Drillon), Wiley-VCH, **2001**; c) *Supramolecular Engineering of Synthetic Metallic Materials* (Eds.: J. Veciana, C. Rovira, D. B. Amabilino,) NATO ASI Series, *Vol. 518*, **1998**
[17] a) J. Veciana, J. Cirujeda, C. Rovira, J. Vidal-Gancedo, *Adv. Mater.* **1995**, *7*, 221; b) E. Hernàndez, M. Mas, E. Molins, C. Rovira, J. Veciana, *Angew. Chem.* **1993**, *105*, 919. *Angew. Chem. Int. Ed. Engl.* **1993**, *32*, 882; c) J. Cirujeda, L. E. Ochando, J. M. Amigó, C. Rovira, J. Rius, J. Veciana, *Angew. Chem.* **1995**, *107*, 99. *Angew. Chem. Int. Ed. Engl.* **1995**, *34*, 55; c) M. M. Matsushita, A. Izuoka, T. Sugawara, T. Kobayashi, N. Wada, K. Takeda, M. Ishikawa, *J. Am. Chem. Soc.* **1997**, *119*, 4369; d) A. Caneschi, F. Ferraro, D. Gatteschi, A. Le Lirzin, M. Novak, E. Rentschler, R. Sessoli, *Adv. Mater.* **1995**, *7*, 476; e) F. M. Romero, R. Ziessel, M. Drillon, J. -L. Tholence, C. Paulsen, N. Kyritsakas, J. Fischer, *Adv. Mater.* **1996**, *8*, 826.
[18] a) H. M. McConnell, *J. Chem. Phys.* **1963**, *33*, 1910; b) R. Breslow, B. Jaun, R. Q. Klutiz, C. Z. Xia, *Tetrahedron* **1981**, *37*, 863; c) J. Zhang, M. Baumgarten, *Chem. Phys.* **1997**, *222*, 1.
[19] a) K. E. Vostrikova, D. Luneau, W. Wernsdorfer, P. Rey, M. Verdaguer, *J. Am. Chem. Soc.* **2000**, *122*, 718; b) C. Rancurel, D. B. Leznoff, J.-P. Sutter, S. Golhen, L. Ouahab, J. Kliava, O. Kahn, *Inorg. Chem.* **1999**, *38*, 4753; c) M. Tanaka, K. Matsuda, T. Itoh, H. Iwamura, *Angew. Chem.* **1998**, *110*, 866. *Angew. Chem. Int. Ed.* **1998**, *37*, 810; d) A. Caneschi, D. Gatteschi, P. Rey, *Prog. Inorg. Chem.* **1991**, *39*, 331, and references therein.
[20] a) N. Hirota, S. I. Weisssman, *J. Am. Chem. Soc.* **1964**, *86*, 2538; b) M. Baumgarten, L. Gherghel, T. Wehrmeister, *Chem. Phys. Lett.* **1997**, *267*, 175, and references therein.
[21] B. N. Figgis, E. S. Kucharski, M. Vrtis, *J. Am. Chem. Soc.* **1993**, *115*, 176; and references therein.
[22] Preliminary results were presented in a communication: I. Ratera, D. Ruiz-Molina, J. Vidal-Gancedo, K. Wurst, N. Daro, J.-F. Letard, C. Rovira, J. Veciana, *Angew. Chem.* **2001**, *113*, 933; *Angew. Chem. Int. Ed.* **2001**, *40*, 919.
[23] K. Maeda, E. Fisher, *J. Israel Chem.* **1977**, *16*, 294.
[24] L. Teruel, Ll. Viadel, J. Carilla, Ll. Fajarí, E. Brillas, J. Sane, J. Rius, L. Juliá, *J. Org. Chem.* **1996**, *61*, 6063.
[25] *X-ray structure analysis*: *Crystal data*: $C_{30}H_{16}Cl_8NFe$, monoclinic, space group $P2_1/n$ (no. 14), $a=8.1900(4)$, $b=29.539(2)$, $c=12.1065(4)$ Å, $\beta=91.021(3)$°, $V=2928.4(3)$ Å^3, $Z=4$, $T=218(2)$ K, $\lambda Mo_{K\alpha}=0.71073$ Å, $F(000)=1460$, $\mu=1.269$ mm^{-1}, $\rho_{calcd}=1.656$ g cm^{-3}, brown platelet $0.2\times0.1\times0.015$ mm. *Data collection*: Nonius Kappa CCD, 5879 measured reflections were corrected for Lorentz and polarization. *Structure solution and refinement*: anisotropic refinement on F^2 (SHELXL 93), hydrogen atoms at calculated positions; R values for 361 parameters and 2191 observed reflections [$I>2\sigma(I)$] $R_1=0.0396$ and $wR_2=0.0703$. CCDC-147245 contains the supplementary crystallographic data for this paper. These data can be obtained free of charge via www.ccdc.can.ac.uk/conts/retrieving.html (or from the Cambridge Crystallographic Centre, 12 Union Road, Cambridge CB2 1EZ, UK; Fax: (+44) 1223-336033; or deposit@ccdc.cam.ac.uk).
[26] A systematic search of the Cambridge Crystallographic Structure Database (CSD) revealed the existence of several examples of imino derivatives in which the -H–C=N- group adopts a *trans* configuration. There is no example of the same group adopting a *cis*

configuration. This agrees with the experimental difficulties found in this work in attempts to crystallize the *cis* isomer.

[27] For any HF function: $E_{(TOTAL)}=\sum_{a}^{occ}\varepsilon_a-\frac{1}{2}\sum_{a}^{occ}\sum_{b}^{occ}(\langle ab|ab\rangle-\langle ab|ba\rangle)$, where ε_a are the HF orbital energies and *a* and *b* are indices which identify spin orbitals (See, A. Szabo, N. S. Ostlund, *Modern Quantum Chemistry*, Macmillan, New York, **1982**, p. 125). As a consequence, there are cases where the value of the bielectronic $\langle ab|a-b\rangle-\langle ab|ba\rangle$ integrals can change the order of the $E_{(TOTAL)}$ given by the sum of the orbital energies. This is usually the case in open shell systems with many states in a small energy window, as is the case in transition metal complexes, among others.

[28] The calculations were done at the B3LYP/LANL2DZ level.

[29] R. S. Mulliken, *J. Chem. Phys.* **1955**, *23*, 1833.

[30] These calculations were performed with the model shown in the inset of Figure 6 which lacks of two of the phenyl groups of the triphenylmethyl unit. They have been discarded to lower the computational cost of the rotational barrier, as they are too far away from the ferrocene unit to play any significant role in defining such a barrier. The only noticeable effect that such a change has in the geometry is that the radical unit -$C_\alpha H_2(C_6H_2Cl_2)$- is now coplanar, instead of presenting an out-of-plane dihedral of 49.1° caused by the steric effects produced by the bulky Cl atoms at the *ortho* positions.

[31] For radical **1** we computed the potential energy curve for values of the θ angle at the lower ($\theta=0$–180°) and upper ($\theta=180$–360°) regions, which were found to be nearly symmetric. In order to reduce the computational costs, we only computed half of the potential energy curve for radical **2**, the lower region($\theta=0$–180°).

[32] *Photochemistry and Photophysics, Vol. 2* (Ed.: J. F. Rabek), CRC Press, Boca Raton, **1990**, Chapter 4.

[33] C. Rovira, D. Ruiz-Molina, O. Elsner, J. Vidal-Gancedo, J. Bonvoisin, J.-P. Launay, J. Veciana, *Chem. Eur. J.* **2001**, *7*, 240.

[34] a) D. R. Scott, R. S. Becker, *J. Chem. Phys.* **1962**, *35*, 516; b) D. R. Scott, R. S. Becker, *J. Chem. Phys.* **1962**, *35*, 2246.

[35] In fact, similar intervalence transition bands have already been observed in mixed-valance complexes containing ferrocenylpyridines. See: T.-Y. Liu, Y. J. Chen, C.-C. Tai, K. S. Kwan, *Inorg. Chem.* **1999**, 38, 674.

[36] S. Barlow, H. E. Bunting, C. Ringham, J. C. Green, G. U. Bublitz, S. G. Boxer, J. W. Perry, S. R. Marder, *J. Am. Chem. Soc.* **1999**, *121*, 3715.

[37] J. Armet, C. Veciana, J. Rovira, J. Riera, E. Castañer, J. Molins, C. Rius, S. Miravitlles, J. Olivella, Brichfeus, *J. Phys. Chem.* **1987**, *91*, 5608.

[38] The observation of the hyperfine coupling with ^{14}N nuclei is remarkable, providing evidence that the unpaired electron is not only delocalized in the triphenylmethyl unit but also into the imine group. This fact is expected to enhance the presence of intermolecular magnetic exchange interactions in the case that -CH=N- groups are involved in intermolecular bonds; as it was confirmed by ESR frozen solution experiments for the *cis*-**1** isomer.

[39] O. Elsner, D. Ruiz-Molina, J. Vidal-Gancedo, C. Rovira, J. Veciana, *Chem. Comun.* **1999**, 579.

[40] I. Ratera, D. Ruiz-Molina, F. Renz, J. Ensling, K. Wurst, C. Rovira, P. Gütlich, J. Veciana, *J. Am. Chem. Soc.* **2003**, *125*, 1462–1463.

[41] The $|D'|$ parameter reflects primarily the mean distance between the interacting electrons and the $|E'|$ parameter depends mostly on the symmetry of the spin density distribution.

[42] The simulation was carried out by superposition of two spectra, one characteristic of a symmetric triplet species, from where the absolute values of the zero-field splitting parameters were obtained, and another consisting of a single broad line characteristic of a monoradical species, which is associated to the fraction of the radicals that remain in solution as monomers (4%).

[43] S. D. Mcglynn, T. Azumi, M. Kinoshita in *Molecular Spectroscopy of the Triplet State*, Prentice Hall, New Jersey, **1969**.

[44] Such delocalization is in agreement with the observation of the hyperfine coupling with ^{14}N nuclei for radical *trans*-**1**, providing evidence that the unpaired electron is not only delocalized in the triphenylmethyl unit but also into the imine group. This fact is expected to enhance the presence of intermolecular magnetic exchange interactions within the -C=N- groups involved in the intermolecular bonds.

[45] R. L. Carlin, *Magnetochemistry*, Springer, Berlin, **1986**, *71*.

[46] *trans*-**1**→*cis*-**1** isomerization was photoinduced for radical **1** using an irradiation lamp with an interference filter centered at 415 nm (bandwidth 60 nm). No evidence of *cis*-**1**→*trans*-**1** isomerization was observed by using various interference filters (centered from 350 to 450 nm).

[47] This fact is an indication of the larger degree of conjugation for isomer *trans*-**1** over isomer *cis*-**1**.

[48] N. R. King, E. A. Whale, F. J. Davis, A. Gilbert, G. J. Mitchell, *J. Mater. Chem.* **1997**, *7*, 625.

[49] It is worth noting that at 20°C in a degassed solution and in the dark both isomers are stable for more than five hours.

[50] M. J. S. Dewar, E. G. Zoebisch, E. F. Healy, J. J. P. Stewart, *J. Am. Chem. Soc.* **1985**, *107*, 3902.

[51] C. Zou, M. S. Wrighton, *J. Am. Chem. Soc.* **1990**, *112*, 7578.

Received: June 2, 2003
Revised: July 31, 2003 [F5194]